UvA-DARE (Digital Academic Repository)

Unbiased image reconstruction as an inverse problem

Pijpers, F. P.

Link to publication

Citation for published version (APA):
Pijpers, F. P. (1999). Unbiased image reconstruction as an inverse problem. *Monthly Notices of the Royal Astronomical Society*, *307*(3), 659-668. https://doi.org/10.1046/j.1365-8711.1999.02680.x

Unbiased image reconstruction as an inverse problem

F.P. Pijpers

Theoretical Astrophysics Center, Institute for Physics and Astronomy, Aarhus University, Ny Munkegade,
8000 Århus C, Denmark

ABSTRACT

An unbiased method for improving the resolution of astronomical images is presented. The strategy at the core of this method is to establish a linear transformation between the recorded image and an improved image at some desirable resolution. In order to establish this transformation only the actual point spread function and a desired point spread function need be known. Any image actually recorded is not used in establishing the linear transformation between the recorded and improved image.

This method has a number of advantages over other methods currently in use. It is not iterative which means it is not necessary to impose any criteria, objective or otherwise, to stop the iterations. The method does not require an artificial separation of the image into "smooth" and "point-like" components, and thus is unbiased with respect to the character of structures present in the image. The method produces a linear transformation between the recorded image and the deconvolved image and therefore the propagation of pixel-by-pixel flux error estimates into the deconvolved image is trivial. It is explicitly constrained to preserve photometry and should be robust against random errors.

Key words: methods : data analysis - methods : numerical - techniques : image processing

1 INTRODUCTION

In astronomy the problem of correcting images for imperfect telescope optics, atmospheric turbulence and other effects that adversely influence the image quality is very well known. There exist therefore many different ways to improve on images or imaging techniques in order to obtain more detailed spatial information. First of all there are hardware based solutions such as adaptive optics and interferometry. It is of course always desirable to make use of such techniques whenever possible. However, given a recorded image with a known point spread function (PSF) and an estimate of the point by point error it is still possible to improve on the spatial resolution by means of software : numerical image deconvolution.

A number of algorithms already exist that attempt to do this image reconstruction. Best known in the field of interferometry at radio wavelengths are probably the CLEAN method (Högbom, 1974 ; Schwarz, 1978 ; Wakker & Schwarz, 1988) and the maximum entropy method (MEM) (cf. Narayan & Nityananda, 1986). For the deconvolution of optical images the Richardson-Lucy (RL) method is well known (cf. Richardson, 1972 ; Lucy, 1974, 1992, 1994). Quite recently a new method was presented by Magain, Courbin, & Sohy (MCS, 1998). A characteristic of all of these methods is that images are reconstructed by placing flux (MEM and RL), or building blocks such as point sources (MCS,

CLEAN, two channel RL) in the field of view and minimizing the difference between the image of this model (after convolution with the PSF) and the actual image. Since this is an inverse problem the solution is generally not unique and it can be quite sensitive to errors in the data. Thus in the minimization there is some need for regularization which is usually a smoothness constraint. The various method differ in which building blocks are used and in the form of regularization applied.

It is however somewhat unsatisfactory to proceed in this manner since astronomical images are not generally easily described by just point sources or objects of a certain shape or size, and may not conform to the smoothness constraint applied. Forcing an algorithm to nevertheless build the image up within such constraints may well introduce an undesirable bias. For this reason it is useful to consider an alternative that does not assume anything about properties of the image in the deconvolution. In fact the method presented here does not even use the image actually recorded until its very last step.

The method of subtractive optimally localized averages (SOLA) was originally developed for application in the field of helioseismology (cf. Pijpers & Thompson, 1992, 1994) to determine internal solar structure and rotation. Since then it has also been successfully applied to the reverberation mapping of the broad line region of active galactic nuclei (AGN) (Pijpers & Wanders, 1994). Instead of operating on

the image, the SOLA method uses the PSF with which the image was recorded. With this PSF and a user-supplied desired PSF a linear transformation is constructed between any recorded image for which that PSF applies and its deconvolved counterpart. The resolution that can be attained in this way is only limited by the sampling of the recording device (the pixel size of the CCD) and by the level of the flux errors in the recorded image. Since the transformation is linear, it is quite straightforward to impose photometric accuracy. Astrometric accuracy at the pixel scale is similarly guaranteed since there is no 'positioning of sources' in the image by the algorithm. Sub-pixel accuracy, claimed for some deconvolution methods, implies subdividing each pixel into subpixels. It requires knowledge of the PSF at very high accuracy and very small errors in the data in order to deconvolve down to a sub-pixel scale. If such information is available the SOLA method can easily accommodate sub-pixel scale deconvolution, without substantial modifications. In what follows however, it is assumed that a single pixel is the smallest scale required.

In section 2 the SOLA method is presented. In section 3 the method is applied to an example image to demonstrate the workings of SOLA. In section 4 the method is applied to some astronomical images. Some conclusions are presented in section 5.

2   THE SOLA METHOD

2.1   arbitrary PSFs

The strategy of the SOLA method in general is to find a set of linear coefficients c which, when combined with the data, produce a weighted average of the unknown convolved function under the integral sign, where the weighting function is sharply peaked. In the application at hand this means finding the linear transformation between an image recorded at a given resolution and an image appropriate to a different (better) resolution.

The relation between a recorded image D and the actual distribution of flux over the field of view I is :

$$D(x,y) = \int dx'dy' \ K(x',y' \ ;x,y)I(x',y') \tag{1}$$

where K is the PSF. If one assumes that the PSF is constant over the field of view then :

$$K(x',y' \ ;x,y) \equiv K(x-x',y-y') \tag{2}$$

Of course generally D is not known as a continuous function of (x,y), but instead it is sampled discretely as for instance an image recorded on a CCD. Thus one has as available data the recorded pixel-by-pixel values of flux $D(x_i,y_j)$. These measured fluxes will usually be corrupted by noise and thus the discretized version of equation (1) is :

$$D_{ij} = \int dx'dy' \ K_{ij}(x',y')I(x',y') + n_{ij} \tag{3}$$

where now K_{ij} refers to the PSF appropriate for the pixel at (x_i,y_j) and D_{ij} is the flux value recorded in that pixel. In the vocabulary usual for the SOLA method the K_{ij} are referred to as integration kernels.

In the SOLA technique a set of linear coefficients c_l is sought which, when combined with the data, produces a

value for the flux R in any given pixel that would correspond to an image recorded with a much narrower PSF. Writing this out explicitly and using (3) yields :

$$R \equiv \sum c_l D_l =$$
$$\int dx'dy' \ \left\{ \sum c_l K_l(x',y') \right\} I(x',y') + \sum c_l n_l \tag{4}$$

in which the double subscript ij has been replaced by a single one l for convenience. Thus one would construct the c_l such that the averaging kernel $\mathcal{K}$ defined by :

$$\mathcal{K}(x',y') \equiv \sum c_l K_l(x',y') \tag{5}$$

is as sharply peaked as possible. If one does this for all locations on the CCD the collected values R_m are then the fluxes corresponding to the image at this (better) resolution with a (improved) "point spread function" $\mathcal{K}$. The so-called propagated error, the error in the flux R is :

$$\sigma_R^2 \equiv \sum \sum c_l c_m N_{lm} \tag{6}$$

Here the N_{lm} is the error variance-covariance matrix of the recorded CCD images where both l and m run over all (i,j) combinations of the pixel coordinates. If the errors are uncorrelated between pixels then (6) reduces to :

$$\sigma_R^2 = \sum c_l^2 \sigma_l^2 \tag{7}$$

which is trivially computed once the coefficients c_l are known.

Ideally one would wish to construct an image corresponding to an infinitely narrow PSF : a Dirac delta function. In practice this cannot be achieved with a finite amount of recorded data. As has already been pointed out by Magain et al.(1998) one must in the deconvolved image still satisfy the sampling theorem. A further restriction arises because of the noise term in equation (3). As is well known in helioseismology the linear combination of data corresponding to a very highly resolved measurement usually bears with it a very large propagated error. In order to obtain a flux value for each pixel in the deconvolved image that does not have an excessively large error estimate associated with it, one needs to remain modest in the resolution sought for in the deconvolved image.

Finding the optimal set of coefficients taking these limitations into account can be expressed mathematically in the following minimization problem. One needs to minimize for the coefficients c_l the following :

$$\int dxdy \ [\mathcal{K} - \mathcal{T}]^2 + \mu \sum \sum c_l c_m N_{lm} \tag{8}$$

Here μ is a free parameter which is used to adjust the relative weight given to minimizing the errors in the deconvolved image and to producing a more sharply peaked kernel $\mathcal{K}$. The higher the value of μ the lower this error but the less successful one will be in producing a narrow PSF. In SOLA one is free to choose the function $\mathcal{T}$. A common choice in SOLA applications is a Gaussian :

$$\mathcal{T} = \frac{1}{f\Delta^2} \exp\left[-\left(\frac{(x-x_0)^2 + (y-y_0)^2}{\Delta^2}\right)\right] \tag{9}$$

Here (x_0,y_0) is the location for which one wishes to know the flux at the resolution corresponding to the width Δ. f

is a normalization factor chosen such that :

$$\int \mathrm{d}x\mathrm{d}y \ \mathcal{T} \equiv 1 \qquad (10)$$

although any set of locations (x_0, y_0) can be chosen, a natural choice in the application at hand is to take all original pixel locations (x_i, y_j). If one wishes to deconvolve to sub-pixel scales this can be done by an appropriate choice of the (x_0, y_0) and Δ.

In terms of an algorithm the problem of minimizing the function (8) leads to a set of linear equations :

$$A_{lm}c_l = b_m \qquad (11)$$

The elements of the matrix A are given by :

$$A_{lm} \equiv \int \mathrm{d}x\mathrm{d}y \ K_l(x,y)K_m(x,y) + \mu N_{lm} \qquad (12)$$

The elements of the vector b are given by :

$$b_m \equiv \int \mathrm{d}x\mathrm{d}y \ \mathcal{T}(x,y)K_m(x,y) \qquad (13)$$

Writing out the dependencies on the free parameters explicitly, determining the coefficients c_l results from a straight-forward matrix inversion :

$$c_l(x_0, y_0 \ ; \Delta, \mu) = A_{lm}^{-1}(\mu)b_m(x_0, y_0 \ ; \Delta) \qquad (14)$$

It is clear that for each point (x_0, y_0) there is a separate set of coefficients c_l which will depend on the resolution width Δ required and on the error weighting μ. Note that it is not necessary to invert a matrix for every location (x_0, y_0), which would certainly be prohibitive if one wishes to calculate the entire deconvolved image. For a given error weighting μ one needs to invert A only once. Only the elements of the vector b need be recomputed for different locations or different resolutions.

In order to ensure that at every point in the reconstructed image the summed weight of all measurements is equal and thus a true (weighted) average it is necessary to additionally impose the condition :

$$\sum c_l \equiv 1 \qquad (15)$$

It is this condition that imposes photometric accuracy on the reconstructed image. Using the method of Lagrange multipliers this condition is easily incorporated into the matrix equation (11) by augmenting the matrix A with a row and column of 1's, and a corner element equal to 0. The vector b gains one extra element equal to 1 as well. The details of this procedure can be found in Pijpers & Thompson (1992, 1994).

2.2   translationally invariant PSFs

Although the method described above can work in principle with general PSFs K, the matrix inversion becomes intractable very quickly as the number of pixels increases. For an image of $M \times M$ pixels the number of elements in the matrix A is $M^2 \times M^2$. The matrix A is symmetric but even so a naive matrix inversion routine would require a number of operations scaling as M^6.

However the entire procedure for obtaining the transformation coefficients for all locations of the CCD can be speeded up considerably if one accepts some restrictions for the properties of the PSF K and of the expected errors N_{lm}. The first restriction is to assume that the PSF is constant over the field of view, that is to say that equation (2) is valid. When condition (2) is met one can easily demonstrate that in equation (12) the integrals of the cross products of the PSFs are a convolution :

$$\int \mathrm{d}x\mathrm{d}y \ K_l(x,y)K_m(x,y) \equiv$$

$$\int \mathrm{d}x\mathrm{d}y \ K(x - x_{i_l}, y - y_{j_l})K(x - x_{i_m}, y - y_{j_m}) \qquad (16)$$

$$= \int \mathrm{d}x'\mathrm{d}y' \ K(x',y')K'(\Delta x_{i_m \, i_l} - x', \Delta y_{j_m \, j_l} - y')$$

in which :

$$K'(x - x', y - y') \equiv K(x' - x, y' - y)$$
$$\Delta x_{i_m \, i_l} \equiv x_{i_m} - x_{i_l} \qquad (17)$$
$$\Delta y_{j_m \, j_l} \equiv y_{j_m} - y_{j_l}$$

Evaluating all the M^4 elements of the matrix A is much simplified by doing this two-dimensional convolution as a multiplication in the Fourier domain. This calculation is then dominated by the FFT calculation which requires $\mathcal{O}(M^2 \log(M))$ operations. Similarly the vectors b in (13) can be evaluated for all locations (x_i, y_j) with a single two-dimensional convolution of K and T, again dominated by the FFT.

If the CCD pixels are assumed to be equally spaced the matrix A for $\mu = 0$ can be constructed in such a way that it becomes of a special type known as symmetric block circulant with circulant blocks (BCCB), for which very fast inversion algorithms exist. Circulant matrices have the property that every row is identical to the previous row, but shifted to the right by one element. The shifting is 'wrapped around' so that the first element on each row is equal to the last element of the previous row. Thus the main diagonal elements are all equal and on every diagonal parallel to the main diagonal of the matrix all elements are equal as well. A BCCB matrix is a matrix that can be partitioned into blocks in such a way that each row of blocks is repeated by shifting (and wrapping around) by one block in the subsequent row of blocks and each individual block is circulant. It can be shown that circulant matrices can be multiplied and inverted using Fourier transforms, and by extension BCCB matrices can be multiplied and inverted using two-dimensional Fourier transforms. The detailed steps of the algorithm are worked out in the appendix.

The restriction on the matrix N_{lm} is that is must also be a symmetric BCCB matrix for the fast inversion algorithm to work. It is evident that fully optimal results can only be obtained if the full $N^2 \times N^2$ covariance matrix of the errors is used. However, the error correlation function for the pixels is expected to behave similarly to the point spread function in the sense that it is large (in absolute value) for small pixel separations and small for large pixel separations, independently of where on the CCD the pixel is located. It is therefore likely that the error covariance matrix will already be BCCB or be very nearly so. Since its role in the minimization of (8) is to regularize the inversion it is in practice not essential that the exact variance-covariance matrix be used. Experience in using SOLA in other fields has shown that the
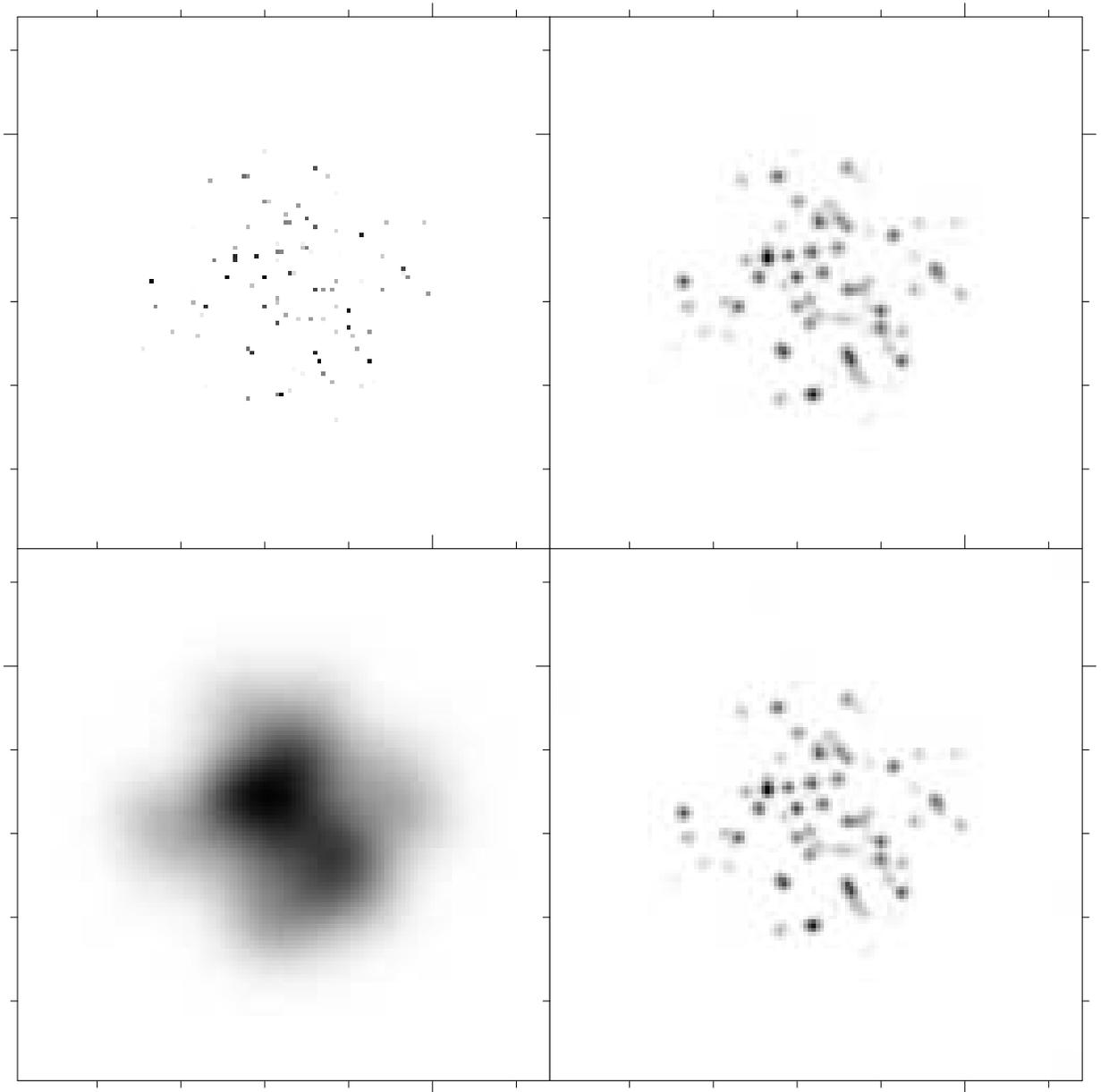
Figure 1. The 128×128 pixels image used in testing the algorithm. Top left panel : the original image. Top right panel : the original convolved with the target PSF : a Gaussian with $\Delta = 1.5$ pixels. Bottom left panel : the original convolved with a PSF which is the sum of a Gaussian with $\Delta = 10$ pixels and an 0.1% contribution from a Gaussian with $\Delta = 1$ pixel. Bottom right panel : the image after SOLA deconvolution of the bottom left image. In all images the grey-scale is linear. In the bottom left image noise is added before deconvolution. In the bottom right image the noise propagated in the deconvolution has an expectation value of ~ 0.5 in arbitrary flux units and the S/N ratio for the brightest pixel is ~ 1000.

results of linear inversions are robust to inaccuracies in the error matrix, as long as those are not orders of magnitude large : if for instance substantial amounts of data (fluxes in pixels) are to be given small weight in the resulting linear combination, because of large errors associated with them, this can give rise to large departures from BCCB behaviour of the error covariance matrix. This would then cause problems for the fast version of the SOLA method presented here. Thus if N_{lm} is not circulant it should in most cases be sufficient to use a BCCB matrix that is close to the original : one

could think of using a modified matrix $\overline{N}_{lm}$ on the diagonals of which are the average values over those diagonals of the true N_{lm}. Of course once the coefficients have been determined, when calculating the propagated errors one should use equation (6) with the proper variance-covariance matrix N_{lm}.

As is shown in the appendix the matrix corresponding to the collection of all vectors of coefficients c, which results from the multiplication of A with the matrix corresponding to the collection of all vectors b (one for every pixel), is also

a BCCB matrix. The process of combining these coefficients c_l with the recorded fluxes on the CCD to form the improved image is :

$$R_{ij} = \sum_k \sum_l C_{kl} D_{i+k-1\,j+l-1} \qquad (18)$$

Since the matrix C is a BCCB matrix and therefore its transpose C^T is as well, the following holds :

$$
\begin{aligned}
R_{ij} &= \sum_{k,\,l} C_{kl} D_{i+k-1\,j+l-1} = \sum_{k,\,l} C^T_{lk} D_{i+k-1\,j+l-1} \\
&= \sum_{k,\,l} C^T_{2-k\,2-l} D_{i+k-1\,j+l-1} \qquad (19) \\
&= \sum_{k',\,l'} C^T_{k'\,l'} D_{i+1-k'\,j+1-l'}
\end{aligned}
$$

From the final equality in (19) it is clear that the process of combining the matrix of coefficients with the image is a convolution, and hence can also be done using FFTs.

From the above it is clear that limiting the algorithm to the case of a PSF that is constant over the CCD implies a profound reduction of the computing time. If the PSFs K satisfy the condition (2) the vectors b collected together for all $(x_0, y_0) = (x_i, y_j)$ form a BCCB matrix, and therefore the matrix inversion of A **and** its subsequent multiplication with **all** vectors b, shown in equation (14), can be done in $\mathcal{O}(M^2 \log(M))$ operations. The entire deconvolved image is thus produced in $\mathcal{O}(M^2 \log(M))$ operations. This acceleration of the algorithm over the version described in the previous section is so substantial that even when the PSF is not constant over the CCD it is worthwhile subdividing the image into subsections in which the PSF can be closely approximated by a single function K. The error introduced in this way can be estimated in a way similar to what is done in the application of SOLA to the reverberation mapping of AGN (Pijpers & Wanders, 1994), and should generally be much smaller than the propagated error from equation (6). If such a subdivision is undesirable, there is the possibility of reverting to the more general algorithm of section 2.1. For a single peaked PSF the matrix A should have a banded structure to which fast sparse matrix solvers can be applied. In this case one could use the inverse of the matrix A for an approximated PSF that is translationally invariant as a pre-conditioner to speed up the matrix inversion for the case of the true PSF.

3   APPLICATION TO A TEST IMAGE

3.1   constructing a narrow PSF

In the first instance it is useful to test the algorithm on a test image for which the result and the errors are known. To this end an artificial image of a cluster of stars is convolved with two different PSFs. One PSF is a sum of two Gaussians ; one with a width $\Delta = 10$ pixels in which 99.9% of the flux is collected, and a second one with a width $\Delta = 1$ pixels which collects the other 0.1% of the flux. Poisson distributed noise is added to every pixel and this 'dirty' image serves as the image to be deconvolved. The other PSF is a Gaussian with a width $\Delta = 1.5$ pixels which is also the target chosen for the SOLA algorithm. Thus the deconvolved image can be
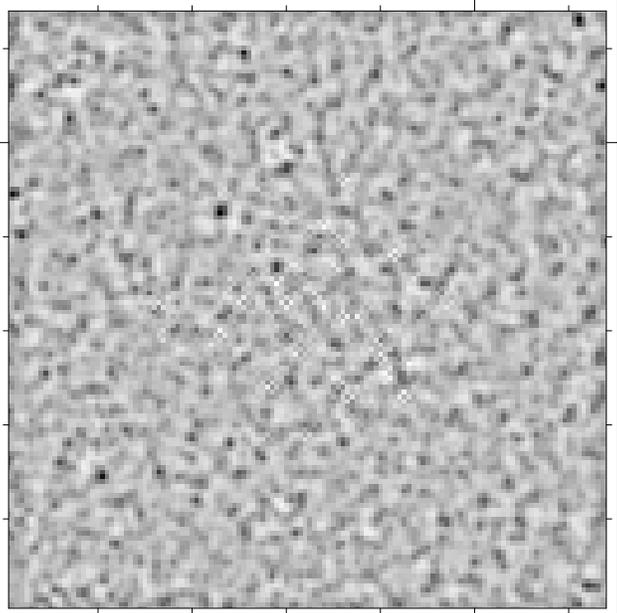

Figure 2. The difference between the image that is SOLA deconvolved and the original image convolved to the target PSF. The gray scale is adjusted so that the full scale is $0.01\times$ the scale in the right-hand side images of figure 1, which corresponds to 10σ of the noise in the deconvolved image.
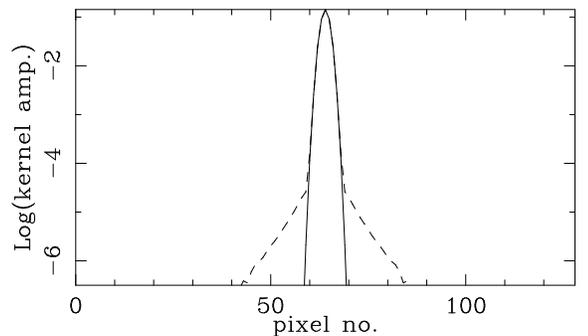

Figure 3. A slice through the peak of the target PSF specified in the SOLA algorithm (solid line) and the averaging kernel $\mathcal{K}$ (dashed) constructed from the linear combination of the pixel PSFs.

compared directly with the image obtained from direct convolution of the original with the narrow target PSF. The results are shown in figure 1. In order to get an optimal reproduction of the target PSF, the error weighting parameter μ is chosen to be equal to 0.

It is clear that the bottom and top right panels are very similar and thus the image appears to be recovered quite well. To illustrate this further the two images can be subtracted. Figure 2 shows the SOLA deconvolved image minus the image convolved with the target PSF, with an adjusted gray scale to bring out the differences, which in the central portion of the image are all < 1%. Although there is no strong evidence for it in this image, the deconvolution
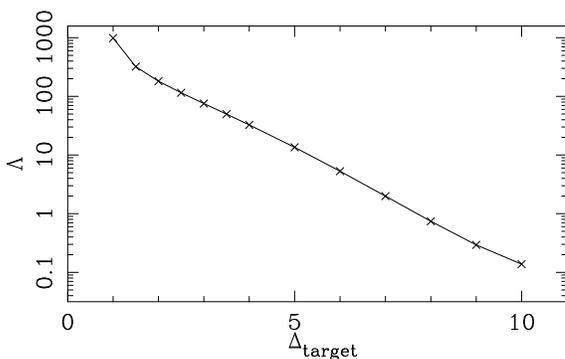
Figure 4. The error magnification Λ as a function of the width Δ of the target PSF specified. The PSF of the blurred image is as described in the text in all cases, the error weighting is $\mu = 0$.

can suffer from edge effects because part of the original image can 'leak away' in the convolution with the broad PSF. When deconvolving, the region outside the image is assumed to be empty and so a spurious negative signature is then introduced in the image. The magnitude of such edge effects must clearly depend both on the image and on the PSF of the 'dirty' image, since they are determined by the information that has been lost at the edges of the CCD. Of course it is desirable to demonstrate this method on a more realistic suite of images than just the simple one used here, which is work currently in progress.

The averaging kernel that is constructed cannot in general match perfectly the target form, even in the absence of errors. In general any function can be completely reconstructed only out of a *complete set* of base functions. Since function space is infinite dimensional this would require an infinite number of base functions. In this test image there are no more available than the 128^2 PSFs corresponding to each of the pixels and so there can never be a perfect matching of $\mathcal{K}$ with $\mathcal{T}$. In figure 3 a section through the maximum of both $\mathcal{T}$ and $\mathcal{K}$ is shown. It is clear that at the 10 ppm level, the constructed averaging kernel starts getting wider than the target. If the ratio of the widths of the target form and actual PSF is even smaller than for this image, alternating negative and positive side lobes can show up in the averaging kernel which cause ringing. The amplitude of the sidelobes, and the width Δ below which ringing starts occurring, will in general depend on the weighting of the errors μ, as has been demonstrated from the application of SOLA to helioseismology (Pijpers & Thompson, 1994).

As it stands the SOLA algorithm does not impose positivity on the image. One could attempt to use a positivity constraint to extrapolate the image beyond the recorded edges in such a way that it eradicates any negative fluxes in the image, which would in principle also remove associated positive artifacts around the edges. However, in the presence of errors this might be somewhat hazardous. Furthermore, in the presence of errors any edge effects might well disappear into the noise.

If one assumes that the covariance of errors between pixels is equal to 0 and the flux error in each pixel is equal to σ^2, or $N \equiv \sigma^2 I$, then it is particularly simple to calculate the flux error for each pixel in the deconvolved image from
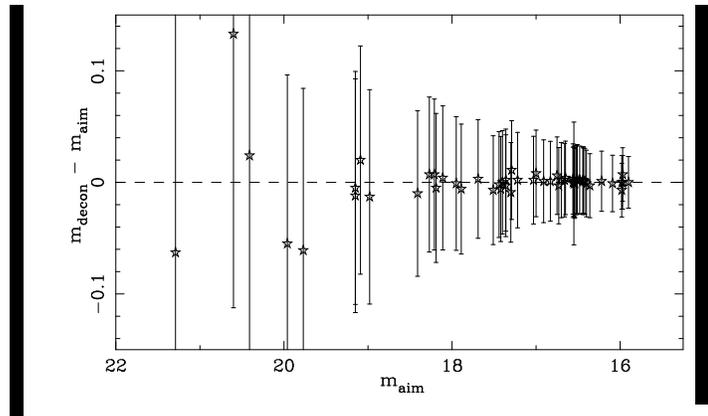

Figure 5. The difference on an arbitrary magnitude scale between the magnitude of the stars in the deconvolved image m_{decon} and the magnitude m_{aim} of their counterparts in the reference image constructed by convolving the original with the target PSF.
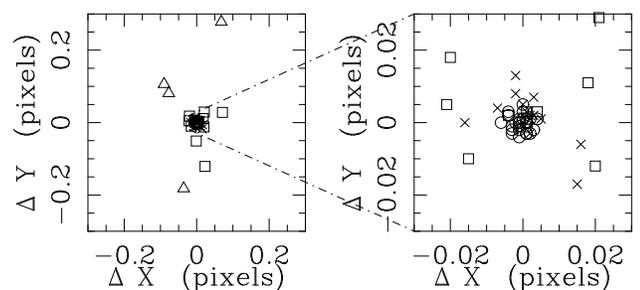

Figure 6. The position difference in pixel units between the stars in the deconvolved image m_{decon} and their counterparts in the image constructed by convolving the original with the target PSF. Open circles : all stars with magnitudes between 15.9 and 16.9, crosses : stars with magnitudes between 16.9 and 17.9, open squares : stars with magnitudes between 17.9 and 18.9, open triangles : all stars with magnitude greater than 18.9.

equation (7) since it is

$$\sigma_R^2 \; = \; \sigma^2 \sum c_l^2 \; \equiv \; \Lambda^2 \sigma^2 \tag{20}$$

This factor Λ is usually referred to as the error magnification and is equal for all pixels in the reconstructed image. In general Λ increases as the ratio of $\Delta_{\mathrm{target}}/\Delta_{\mathrm{PSF}}$ decreases. For the deconvolved image of figure 1 the error magnification is ~ 321. The magnitude of the error magnification for this simple example illustrates that the true limitation of deconvolving images may in practice not lie in the sampling theorem, but instead in the S/N of the recorded image. For example for a point source the peak flux in its central pixel will increase in the deconvolution by a factor which is roughly $\mathrm{FWHM}_{\mathrm{PSF}}/\mathrm{FWHM}_{\mathrm{target}}$. The noise will increase by a factor Λ and so the signal-to-noise ratio for point sources will scale roughly as :

$$\left(\frac{S}{N}\right)_{\mathrm{decon}} \approx \frac{1}{\Lambda} \left(\frac{\mathrm{FWHM}_{\mathrm{PSF}}}{\mathrm{FWHM}_{\mathrm{target}}}\right) \left(\frac{S}{N}\right)_{\mathrm{dirty}} \tag{21}$$

Thus in the example shown the signal-to-noise ratio for point sources is degraded by a factor of roughly ~ 48 between the dirty image and the deconvolved image. This clearly requires a very high a signal-to-noise ratio in the dirty image, which means that in practice as dramatic a resolution enhancement

as attempted here will not usually be possible. A more modest resolution enhancement of around a factor of 2 should in most cases be possible however, as can be deduced from figure 4.

In order to show the relation between resolution and error magnification in figure 4 is shown the value of the error magnification as a function of the width Δ specified for the target function. If only the broad component had been present the error magnification would have been unity for a target $\Delta = 10$. Effectively because of the narrow component which captures a mere 0.1% of the flux the image can be deconvolved to a PSF with $\Delta = 8$ pixels without significant penalty in the magnification of the errors.

The CPU time used to construct the matrix A, all the vectors b, to invert A and multiply with all b and finally to combine the coefficients with the image takes ~ 0.5 min on an SGI workstation for this 128×128 image.

3.2 photometric and astrometric accuracy

Since there is no placement of flux or point sources, the algorithm should automatically be astrometrically accurate. Photometric accuracy is ensured by explicitly constraining the linear coefficients to sum to unity, i.e. imposing constraint (15). In order to demonstrate both these properties for this test image a standard photometric package DAOPHOT was used to do aperture photometry on the deconvolved image, and on the image obtained by convolving the original with the target PSF. The deconvolved image of course has noise propagated from the dirty image. The other image is kept noise-free to properly serve as a reference. The errors are calculated by DAOPHOT and are consistent with what is expected from the noise in the deconvolved image. In figure 5 is shown the difference between the magnitudes of the stars in the two images as a function of the stellar magnitudes in the reference image. The difference is clearly consistent with zero over the entire range of 5 magnitudes, and does not show any trend.

DAOPHOT calculates the error bar assuming that the error in different pixels is uncorrelated. For the SOLA deconvolved image this is not the case. In the deconvolved image the error correlation function falls below 0.01 in absolute value only at inter-pixel distances larger than ~ 12 for this test case. Furthermore, because fluxes are combined with positive and negative coefficients, the error is not distributed as for a Poisson process. If this is taken into account properly the error bars in figure 5 should be decreased and are then compatible with the actual scatter of the points.

DAOPHOT also determines the positions of point sources in the image and therefore those positions can be used to determine astrometric accuracy. In figure 6 are shown the difference in units of a pixel between the DAOPHOT determined positions in the two images. Here the stars have been grouped into 4 magnitude bins, each bin 1 magnitude in range, and starting from the brightest star with magnitude 15.9. The right-hand panel is a blow-up of the central portion of the left-hand panel. Figure 4 shows that there is a trend in that the fainter stars show a greater scatter in position, the largest position difference being of the order of ~ 0.2 pixels. In the right-hand panel it can be seen that for stars brighter than magnitude 19 the difference in positions is smaller than 0.03 pixels. These
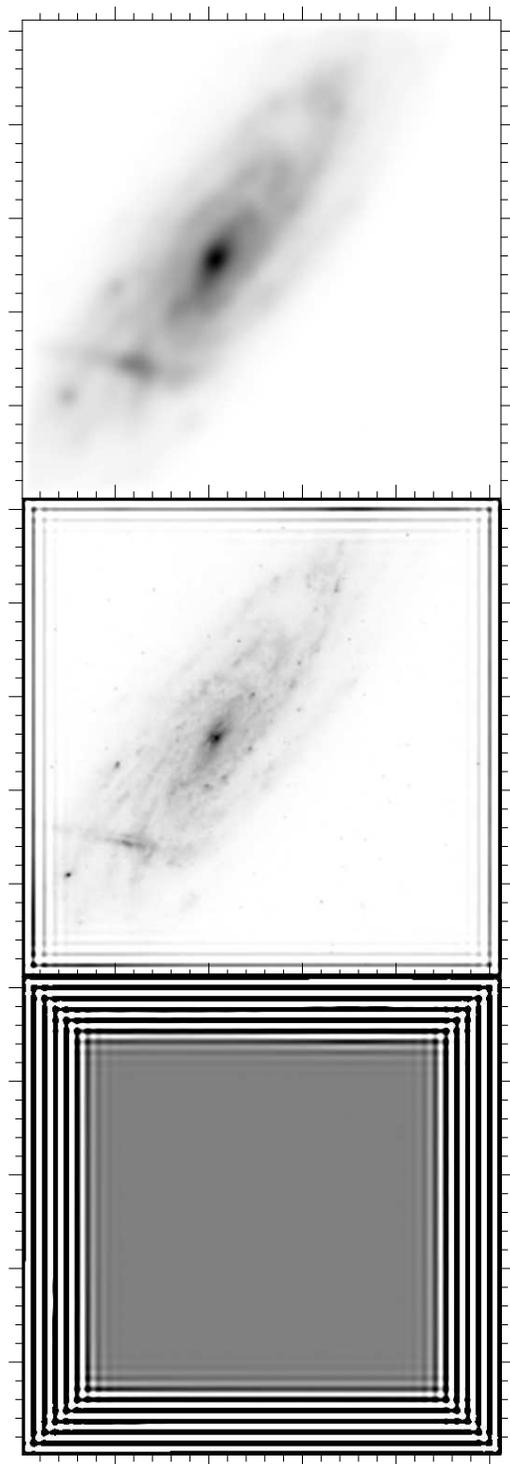

Figure 7. Images of the galaxy UGC 5041. The top image is convolved with the same broad PSF used on the image at the bottom left in figure 1. The middle image is the deconvolved image with a PSF with a FWHM of 2.5. The bottom image is the difference between the original image convolved with the target PSF, and the deconvolved image, no noise has been added. The gray scale of the bottom panel extends between $\pm 0.1\%$ of the gray scale of the middle image.
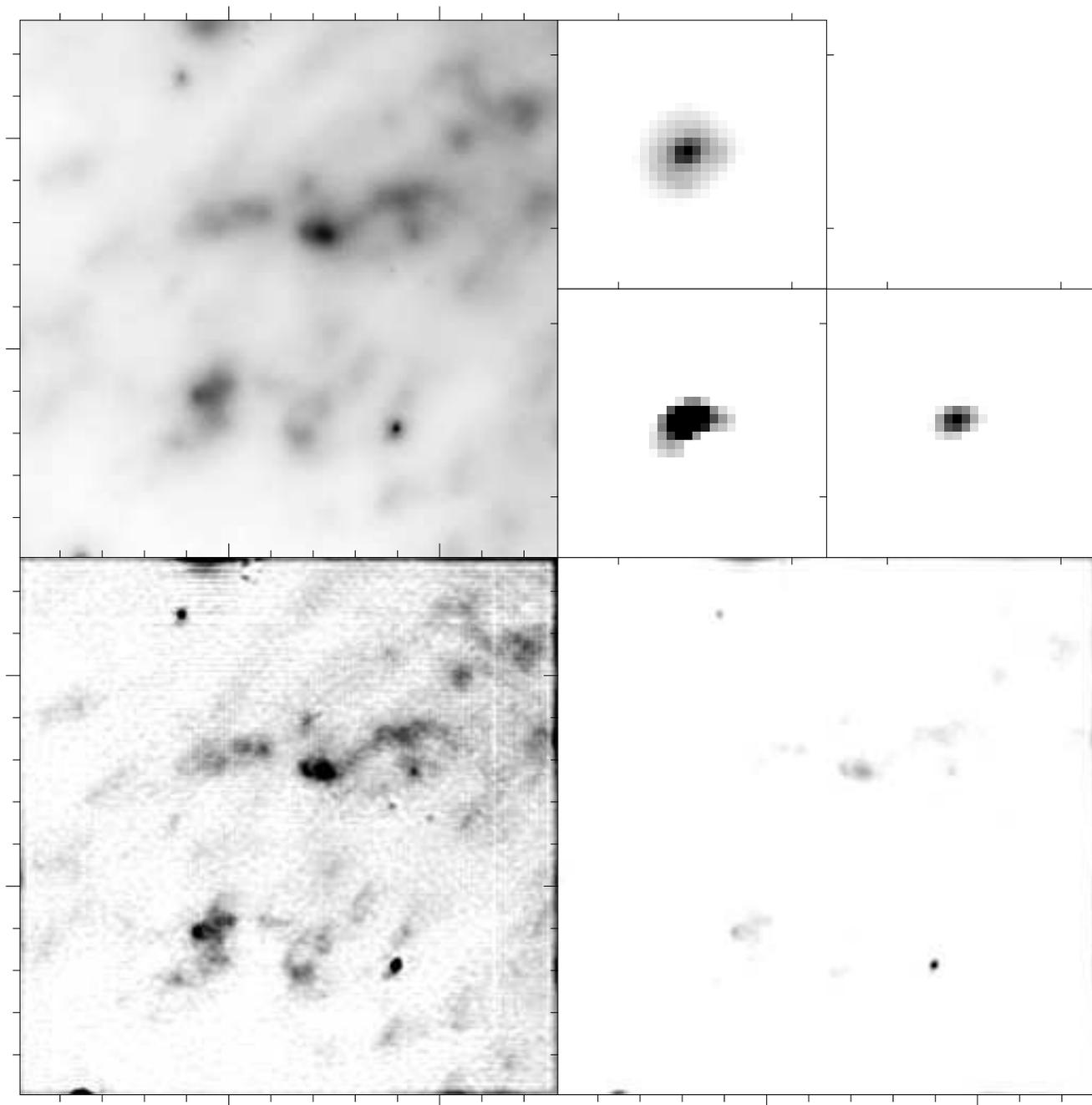
Figure 8. Image of a detail of the Orion Molecular Cloud obtained using adaptive optics in IR lines of shocked molecular hydrogen, north is at the top of the image, east is to the left. The image size is 256×256 pixels at 50mas/pixel. The top left image is as obtained with the Adonis instrument on ESO's 3.6m telescope. The PSF for this image is shown on a $4\times$ enlarged scale as the 32×32 pixel image in the top left-hand corner of the top right-hand panel. The bottom left- and right-hand panels are the deconvolved image using different gray-scales. The two bottom images in the top right-hand panel show 32×32 pixels images of the PSF for the deconvolved image, using the same gray scales as the corresponding images, and the same spatial scale as the PSF for the original. For all images the dynamic range between lightest and darkest colour is a factor of ~ 8 in flux level.

uncertainties are entirely consistent with the accuracy with which DAOPHOT can determine stellar positions.

From figures 5 and 6 it is clear that if any errors in photometry or in position are introduced by the deconvolution process, they are much smaller than the errors due to the random noise.

4 APPLICATION TO ASTRONOMICAL IMAGES

4.1 UGC 5041

To give a somewhat more interesting example, a high resolution HST image of a galaxy is blurred and then decon-

volved to demonstrate that the method also works on an image which contains a combination of extended structure and point sources.

The galaxy UGC 5041 is an Sc type galaxy at a redshift of 0.027 (Haynes et al.., 1997). It has been part of various surveys for use in studies of clustering and in establishing distance scales for the Tully-Fisher distance method. In figure 7 is shown a 512×512 image of this galaxy obtained in March 1997 using the WFPC2 (WF3) instrument on board the Hubble Space Telescope (HST) with the F814W filter which corresponds to the I-band. The resolution of the original image has a FWHM of 1.4 pixels and is convolved with the same broad PSF used in the bottom left panel of figure 1. It is then deconvolved to the same resolution as the right-hand images of figure 1 and the result is shown in the middle panel of figure 7. The difference image between this deconvolved image and a reference is shown in the bottom panel of figure 7, where the gray scale is enhanced to demonstrate that in the absence of noise the differences between the deconvolved image and the reference image are less than 0.1% of the peak flux apart from edge effects.

4.2   Orion Molecular Cloud

Observations in IR lines of shocked H_2 of the SE part of the Orion Molecular Cloud complex (OMC1) have been performed at the ESO 3.6m telescope taking advantage of the high spatial resolution given by adaptive optics (Adonis at 50 marcsec/pixel) combined with the high spectral resolution given by a Fabry-Perot (R=1000) (Vannier et al., 1998). The image is deconvolved using a target PSF with FWHM 3 pixels and an error weighting $\mu = 0$. The resulting error magnification factor is $\Lambda = 6.2$. The dynamic range in the deconvolved image is ~ 30 as opposed to ~ 8 in the original. For this reason the deconvolved image is shown twice : bottom left in figure 8 is shown a linear gray scale extending from an estimated noise level to 8 times that, bottom right is shown a linear gray scale extending from the peak level in the deconvolved image which is ~ 30 times the estimated noise level, to 1/8 of that. The PSF of the deconvolved image, i.e. the constructed averaging kernel $\mathcal{K}$, is shown using the same two gray scales in the bottom part of the top right-hand panel of figure 8.

Although some of the 'graininess' in the bottom panels must be due to the increased noise compared to the top left-hand image, fine structure can clearly be seen in the bottom panels of figure 8. There is also some evidence of edge effects at the top and right of the image. From the image of the PSF of the deconvolved image it is also clear that, as expected, the Gaussian target is not reproduced perfectly over the entire dynamic range of the deconvolved image. Comparing the PSF images with the same dynamic range from the peak down (top left and bottom right in the top right-hand panel of figure 8) it is clear that the PSF is indeed much narrower for the deconvolved image.

5   CONCLUSIONS

In this paper the SOLA inversion method, well known in helioseismology, is applied to the reconstruction of astronomical images. It is demonstrated how a linear transformation is constructed between any image recorded with a known PSF

and its deconvolved counterpart with a different (narrower) PSF. The method itself uses **only** the PSF and no assumptions are made concerning what is contained within the image(s) to be deconvolved. It is furthermore shown that in the case of translationally invariant PSFs, a fast algorithm, using $\mathcal{O}(N \log N)$ operations where N is the total number of pixels in the image, can be constructed, which allows deconvolution of even 1024×1024 images within half an hour on medium-sized workstations.

REFERENCES

Haynes M.P, Giovanelli R., Herter T., Vogt N.P., Freudling W., Maia M.A.G., Salzer J.J., Wegner G., 1997, Astron. J. 113, 1197
Högbom J.A., 1974, A&A Supp. 15, 417
Lucy L.B., 1974, Astron. J. 79, 745
Lucy L.B., 1992, Astron. J. 104, 1260
Lucy L.B., 1994, A&A 289, 983
Magain P., Courbin F., Sohy S., 1998, ApJ 494, 472
Narayan R., Nityananda R., 1986, Ann. Rev. A&A 24, 127
Pijpers F.P., Thompson M.J., 1992, A&A 262, L33
Pijpers F.P., Thompson M.J., 1994, A&A 281, 231
Pijpers F.P., Wanders I., 1994, MNRAS 271, 183
Press W.H., Teukolsky S.A., Vetterling W.T., Flannery B.P., 1992, Numerical Recipes, the art of scientific computing 2nd Ed., CUP, Cambridge, 70
Richardson W.H., 1972, J. Opt. Soc. Am. 62, 55
Schwarz U.J., 1978, A&A 65, 345
Vannier L., Lemaire J.-L., Field D., Rouan D., Pijpers F.P., Pineau des Forêts G., Gerin M., Falgarone E., 1998, ESO/OSA Meeting on Astronomy with Adaptive Optics. Present results and future programs, Sonthofen Germany 7-11 sept 98, in press
Wakker B.P., Schwarz U.J., 1988, A&A 200, 312

APPENDIX A: THE INVERSION AND MULTIPLICATION OF CIRCULANT MATRICES

As it stands the matrix described in (16) does not conform to the criteria for a block circulant with circulant blocks (BCCB) matrix. Instead it is a block Toeplitz matrix with Toeplitz blocks. For the latter type of matrix the elements are also identical on diagonals but there is no 'wrapping around' from row to row : the final element of each row is not (necessarily) equal to the first element of the subsequent

row. In order produce a matrix that is a BCCB matrix it is useful to envisage a 'virtual CCD' that is twice as big in both dimensions as the actual CCD, which for convenience is assumed to be square. This 'virtual CCD' has the property that it has a periodic point spread function in both directions : the CCD is shaped like a torus. The actual CCD then occupies one quarter of this virtual CCD and the other three quarters are 'empty sky'.

For this virtual CCD the matrix constructed by (16) is a $(2M)^2 \times (2M)^2$ BCCB matrix. The first quadrant of this matrix, $(M)^2 \times (M)^2$ in size, is identical to the matrix for the actual CCD. Unless explicitly stated otherwise the matrices for this torus-shaped virtual CCD are the ones that the algorithm works on. In what follows the indices 'wrap around' which is to say that the values of the indices are to be evaluated modulo the matrix dimension.

First consider a matrix that is fully circulant rather than block circulant with circulant blocks. Such a matrix A satisfies :

$$A_{i+n\,j+n} = A_{ij} \qquad \forall n, \ (i+n)\mathrm{mod}(M_A),$$
$$(j+n)\mathrm{mod}(M_A) \tag{A1}$$

in which the matrix A has dimensions $M_A \times M_A$. An ordinary matrix multiplication of two circulant matrices A and B satisfies :

$$
\begin{aligned}
C_{ij} &= \sum_k A_{ik}B_{kj} \\
&= \sum_k A_{i+n\,k+n}B_{k+n\,j+n} \\
&= \sum_l A_{i+n\,l}B_{l\,j+n} \qquad \text{with } l \equiv k+n \\
&= C_{i+n\,j+n} \qquad \forall n
\end{aligned}
\tag{A2}
$$

Thus C is circulant if A and B are circulant. It is also straightforward to demonstrate that if A and C are circulant, B must be circulant as well :

$$
\begin{aligned}
0 &= C_{i+n\,j+n} - C_{ij} \\
&= \sum_l A_{i+n\,l}B_{l\,j+n} - A_{il}B_{lj} \\
&= \sum_k A_{ik}\left(B_{k+n\,j+n} - B_{kj}\right) \quad k \equiv l-n
\end{aligned}
\tag{A3}
$$

Since A is an arbitrary circulant matrix the final equality can only lead to 0 (and thus consistency) if B is indeed circulant.

Since the identity matrix is itself a circulant matrix, a direct consequence is that the inverse of any circulant matrix A^{-1} is also circulant, which is trivially demonstrated by substituting I for C.

If the matrix C is circulant then it is fully determined by its first row, as can be demonstrated by taking $n = 1 - i$ in (A2), for which the following holds :

$$
\begin{aligned}
C_{1n} &= \sum_l A_{1l}B_{ln} \\
&= \sum_l A_{1l}B_{1\,n+1-l}
\end{aligned}
\tag{A4}
$$

A one-dimensional convolution of two functions is defined
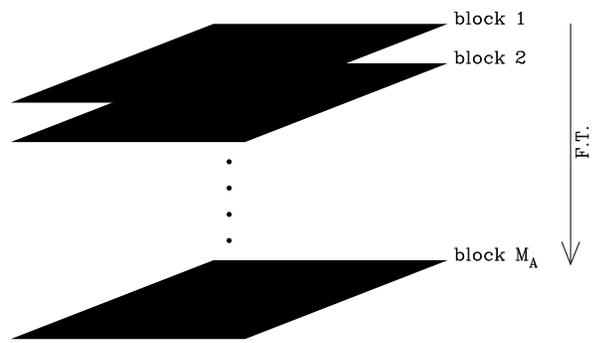

Figure 9. The first row of blocks of a BCCB matrix ar stacked above each other. The first step in multiplying two BCCB matrices is to do a FT on these stacks for each matrix in the direction indicated by the arrow. Since the blocks individually are circulant one only needs to do this for the front face of this cube by performing an FT on each row and multiplying in the Fourier domain.

by the following integral :

$$C(x) = \int \mathrm{d}x' A(x)B(x - x') \tag{A5}$$

which in discretized form is :

$$C_i = \sum_l v_l A_l B_{i+1-l} \tag{A6}$$

where the v_l are integration weights. The v_l can always be arranged to be unity and so it is clear that (A6) and (A4) are identical summations. This means that the multiplication of two circulant matrices can be regarded as a convolution. The product of two circulant matrices can therefore be determined by multiplying the Fourier Transform (FT) of the first row of each of the two matrices, and then taking the inverse FT of this product. This yields only the first row of that product but since it is known to be a circulant matrix the other rows are then trivially found by shifting and wrapping around. Similarly the inverse of a circulant matrix can be found by dividing the FT of the first row of the identity matrix by the FT of first row of the circulant matrix to be inverted, and taking the inverse FT.

If one has a BCCB matrix with dimensions $M_A^2 \times M_A^2$ in which the blocks have dimensions $M_A \times M_A$, it is fully determined by its first row of blocks. In equations (A2)-(A6) it is nowhere used that the individual matrix elements must be scalars. Thus two block circulant matrices can be multiplied by a one-dimensional convolution of the first row of blocks of each matrix, i.e. doing the same operation of convolution on every element of each block. One can visualize this as in diagram 9 by stacking the blocks and doing a one dimensional FT along columns. Since the blocks are circulant it is not necessary to do this operation for all columns. One does M_A one-dimensional FTs along the first rows of the blocks for each matrix and then multiplies row by row these first rows.

The first step is therefore to perform the M_A one dimensional FTs of the first row of each block, for both matrices. The second step is to treat each of these rows as an element in an array, and the two arrays corresponding to matrix A

and B are convolved. The two-level hierarchy of one dimensional FTs can be achieved simply by one two-dimensional FT, in which one direction is a horizontal one and the other the vertical in diagram 9. The two-dimensional FT is thus applied to a matrix of size $M_A \times M_A$ instead of a one dimensional FT on the first row of the full matrix. For a multiplication of two matrices the two-dimensional tableaux are multiplied element by element in the Fourier domain and the result is inverse FT'd. The result is the first row of the BCCB product matrix, where the other rows are obtained by shifting and wrapping around. The inverse of a matrix in the Fourier domain is a simple division and therefore carried out analogously to the multiplication of matrices.

By using FFT algorithms the inversion of block circulant matrices with circulant blocks with size $M \times M$ is thus carried out in $\mathcal{O}(M^2 \log M)$ operations.

One more step is necessary in order to be able to apply this method of inverting matrices to the problem at hand. Because of the constraint (15) the block circulant matrix with circulant blocks is augmented with one row and column. All elements of this row and column are equal to unity except for the corner element which is 0. Thus the matrix to be inverted is A' :

$$A' \equiv \begin{pmatrix} A & \mathbf{1} \\ \mathbf{1}^{\mathrm{T}} & 0 \end{pmatrix} \tag{A7}$$

where A is a BCCB matrix and $\mathbf{1}$ is a column vector of which all M_A^2 elements are equal to 1. The inverse of this partitioned matrix can be written as (cf. Press et al., 1992) :

$$A'^{-1} \equiv \begin{pmatrix} P & Q \\ Q^{\mathrm{T}} & -\frac{1}{s} \end{pmatrix} \tag{A8}$$

in which P has the same dimensions as A, Q is a column vector, and s is a scalar :

$$P = A^{-1} - \frac{1}{s} A^{-1} \cdot \mathbf{1} \cdot \mathbf{1}^{\mathrm{T}} \cdot A^{-1}$$
$$Q = \frac{1}{s} A^{-1} \cdot \mathbf{1} \tag{A9}$$
$$s = \left(\mathbf{1}^{\mathrm{T}} \cdot A^{-1} \cdot \mathbf{1} \right)$$

Since A is a block circulant matrix with circulant blocks the column vector resulting from the product $A^{-1} \cdot \mathbf{1}$ is itself a column vector $\alpha \mathbf{1}$ where α is some number that depends on A. Using this (A9) can be simplified further :

$$P = \left(I - \frac{1}{M_A^2} \mathbf{1} \cdot \mathbf{1}^{\mathrm{T}} \right) \cdot A^{-1}$$
$$Q = \frac{1}{M_A^2} \mathbf{1} \tag{A10}$$
$$s = M_A^2 \alpha$$

The matrix formed by $\mathbf{1} \cdot \mathbf{1}^{\mathrm{T}}$ is clearly a circulant matrix and therefore also block circulant with circulant blocks. The matrix multiplications to evaluate P can therefore be done with FTs as described above.

The first step in this process is sectioning the first rows and rearranging. The $M_A \times M_A$ matrix formed from sectioning and rearranging the first row of I has only one non-zero element which is the first element of the first row (equal to 1). The FT of this matrix is a matrix of which every element is equal to 1. The matrix formed from sectioning and rearranging the first row of $\frac{1}{M_A^2} \mathbf{1} \cdot \mathbf{1}^{\mathrm{T}}$ is an $M_A \times M_A$ matrix of

which every element is equal to $\frac{1}{M_A^2}$ and so the first element of the first row of its FT is equal to 1 and all other elements are 0. Subtracting one from the other in the Fourier domain produces a matrix with as the first element of the first row a 0 and all other elements equal to 1. Evaluating the FT of P and doing the inverse FT is then trivial.

All the vectors b of equation (13) collected for all pixels also form an $M_A^2 \times M_A^2$ BCCB matrix B with one extra bottom row of 1's arising from the constraint (15). The product of this with the A'^{-1} is therefore also most easily carried out in the Fourier domain using P. Adding the final element due to the addition of the element $Q \cdot \mathbf{1}^T$ is a simple addition of $1/M_A^2$ to every element of $P \cdot B$. Since FTs are linear this addition can also be done in the Fourier domain, by setting the first element of the first row of $P \cdot B$ equal to 1 before performing the inverse FT.